PHOTONICS Research

Superior performance of a 2 kHz pulse Nd:YAG laser based on a gradient-doped crystal

Meng'en Wei,[1,2] Tingqing Cheng,[1] Renqin Dou,[3] Qingli Zhang,[3] and Haihe Jiang[1,2,*]

[1]Anhui Province Key Laboratory of Medical Physics and Technology, Center of Medical Physics and Technology, Hefei Institutes of Physical Science, Chinese Academy of Sciences, Hefei 230031, China
[2]University of Science and Technology of China, Hefei 230026, China
[3]Anhui Institute of Optics and Fine Mechanics, Chinese Academy of Sciences, Hefei 230031, China
*Corresponding author: hjiang@aiofm.ac.cn

Received 12 March 2021; revised 9 April 2021; accepted 10 April 2021; posted 13 April 2021 (Doc. ID 424989); published 8 June 2021

Herein, we report a homemade new Nd:YAG crystal rod that contains a gradient dopant of 0.39–0.80 at.% Nd^{3+} from end to end, achieving superior performance of a 2 kHz Nd:YAG pulse laser at 1064 nm. The optical-to-optical conversion efficiency reached 53.8%, and the maximum output power of the laser was 24.2 W, enhanced by 35.9% compared with a uniform crystal rod with the same total concentration of Nd^{3+}. Significantly, our experiments revealed that the gradient concentration crystal produced a relatively even pumping distribution along the rod axis, greatly reducing the temperature gradient as well as having a smaller thermal effect. The pump and thermal distribution smoothing obviously improved the features of laser oscillation and output.

https://doi.org/10.1364/PRJ.424989

1. INTRODUCTION

Pulsed solid-state lasers, which have been widely used, need to further improve their output energy and energy efficiency in order to be successfully used in other energy-limited environments such as aerospace exploration. End-pumped solid-state lasers have proven to be one of the most efficient methods for producing a high repetition rate and good optical beam quality. The end pumping can easily match the mode of the pump beam with the mode of the resonator in the laser cavity, leading to a lower lasing threshold [1,2]. In the case of single-ended pumping, however, traditional uniform dopant crystals will cause the uneven distribution of pumping energy along the propagation direction due to the attenuation of pumping light by the absorption by dopant ions in the crystal rod. The resultant temperature gradient distribution produces a high thermal lensing effect, which obviously decreases the efficiency of the system, the optical beam quality, and the laser stability [3–6]. To help address this problem, some possible approaches have been tried by using low concentrations of Nd^{3+} crystals and dual-ended pumping to reduce the distribution of temperature gradients [7–10]. As a result, however, weak absorbance in low concentrations of Nd^{3+} crystals will reduce the efficiency of pumping light, and the dual-ended pumping makes the equipment very complex to avoid incident light entering another pumping source with possible damage. However, high concentrations of Nd^{3+} crystals will bring about power saturation, serious thermal effects, and possible concentration quenching at strong pump power [11,12]. In the study of an 808 nm CW diode pumped uniformly doped Nd:YAG laser, Kushawaha *et al.* obtained an optical-to-optical conversion efficiency of about 40% in multimode operation, and Frede *et al.* reported an optical-to-optical efficiency of 48% [13,14]. Obtaining both temperature uniformity of gain media and the high efficiency in the use of pumping light is still unsolved challenges.

A stacked structure of the multi-segment Nd:YAG and Nd:YVO_4 crystals with gradually high Nd^{3+} concentration later was adopted as gain media, enhancing the conversion efficiency significantly [15–18]. One of the main reasons is that the stepped-up doping concentration of the stacked structure greatly reduced the absorption of pump light at the input end, enabling the middle and end parts of the crystal to obtain enough pumping energy. However, the key drawbacks are that if stack fabrication is not perfect, the multiple interfaces and the Nd^{3+} concentration jumps in multisegment crystals inevitably result in the reflection of pump light and affect the oscillation and amplification of laser oscillation. In addition, the multisegmented crystal structures were complex, expensive, and susceptible to distortion in stack preparation. Wilhelm *et al.* made the gradient dopant Nd:YAG plus two undoped YAG endcaps to obtain a maximum output power of 187 W in CW mode [15]. Nevertheless, the abovementioned problems of multi-segmented laser crystals still need to be resolved.

In this paper, a modified Czochralski method [19] was used to grow a gradient dopant Nd:YAG crystal that was used to fabricate a high-repetition-rate pulsed laser. To clarify the

thermal and optical mechanism and performance of gradient concentration crystals, thermal imaging revealed the temperature distribution along the rod axis and a small temperature gradient at high-repetition-rate pumping. We have made the theoretical calculation to get the accurate thermal focal lengths of crystal rods and performed measurement verification. For the first time to our knowledge, a pulsed laser experiment with Nd:YAG crystal having a concentration gradient has been carried out. The maximal output laser power and the optical-to-optical conversion efficiency of the gradient concentration crystal was greatly enhanced in comparison with the uniform concentration crystal. The gradient concentration crystal exhibited excellent pulsed laser properties at high-repetition-rate pulse pumping.

2. GROWTH OF THE GRADIENT Nd:YAG CRYSTAL

Growth of single crystals with a constant gradient of impurity concentration is presented using the Czochralski method [20]. In this method, there are two crucibles, one inside the other, and the concentrations of activator in the internal and external crucibles are different. Under conditions of absence of diffusion between these vessels, the concentration of dopant ion in the process of growth of a single crystal will vary according to the rate of movement of the internal crucible, the segregation coefficient of the activators in a single crystal, the geometry of the crucible, and the concentration of activators in both internal and external crucibles. This dual-crucible technology can achieve controllable ion doping concentration by an additional supplement in the external crucible, but the equipment is very complex and the noble metal crucibles are expensive.

In this study, we have developed a single small-volume crucible strategy that combines the advantages of two important methods for crystal growth from high temperature melt, Czochralski and Kyropoulos methods. In the Kyropoulos method, its crystal shoulder is very short, and after the shoulder stage there is no crystal rotation and mechanical pull, and crystal growth speed is equal to melt drop speed, so no mechanical perturbation during isodiametric boule growth, which is beneficial to crystal quality and is widely used in sapphire growth. In the case of the Czochralski method, however, there is crystal rotation and mechanical pull, the crystal growth speed is the sum of mechanical shift and melt drop speed, and the ratio of crystal radius to crucible radius is only ~50% when it is used to grow doped crystal. Rotation can apply a forced convection on melt near the interface between crystal and melt, which is beneficial to the improvement of doped crystal quality. The main characters in our method, which can be called the quasi-Kyropoulos method, are as follows: the pull mechanical speed to the grown crystal at the shoulder stage is gradually decreased, which is like the Czochralski method, and is less than melt drop speed or close to zero until the isodiametric growth stage, which is like the Kyropoulos method.

The dopant concentration variation in crystal can be expressed by the following equation [19]:

$$C_S = C_0 k_{\text{eff}} (1-g)^{k_{\text{eff}}-1}, \tag{1}$$

where C_S is the concentration of doped ion of the grown crystal, C_0 is the concentration of doped ion of the starting material, k_{eff} is the effective segregation coefficient of doped ion in crystal, and g is the crystallization ratio that can be expressed as $g = \frac{W_S}{W_T}$ (W_S is the weight of the grown crystal and W_T is that of the starting material).

Although k_{eff} can be affected by temperature field gradient, rotation speed, crystal growth speed, and so on, these effects are relatively less in our method. For an actual crystal, it can be seen that the concentration difference between the upper and lower parts of the crystal increases with the increase of g, and W_S is determined by the length and diameter of the grown crystal while W_T is determined by the size of crucible used for crystal growth. Under the condition of the same crucible size, the larger the crystal diameter, the bigger the W_S and g are according to Eq. (1), which lead to a larger concentration gradient. During our method, the crystal diameter during the boule stage is close or equal to the limitation diameter $d_{\max}$:

$$d_{\max} = 2\sqrt{\rho_m/\rho_c} R_c, \tag{2}$$

where ρ_m, ρ_c, and R_c are melt density, crystal density, and crucible radius. The desired diameter of crystal growth was set close to $d_{\max}$, the temperature was controlled by an automatic procedure in the Czochraski furnace, and the ratio of crystal radius to crucible radius was 83% in our experiment. Therefore, the Nd concentration in the YAG could be increased rapidly with the crystal growth due to the dopant segregation effect. In this case, the interspace between crystal and crucible wall is very small so that we did not allow the rotation of the growing crystal to avoid rubbing the crucible wall after the shoulder crystal growth.

Nd:YAG crystal was prepared from the high-purity Y_2O_3, Nd_2O_3, and Al_2O_3 according to the chemical reaction

$$1.5(1-x/k_{\text{eff}})Y_2O_3 + 1.5x/k_{\text{eff}}Nd_2O_3 + 2.5Al_2O_3 \rightarrow (Nd_{x/k_{\text{eff}}}Y_{1-x/k_{\text{eff}}})_3Al_5O_{12}, \tag{3}$$

where x is the initial dopant concentration of the crystal and k_{eff} is the effective segregation coefficient. The raw materials were fully mixed and pressed into a disk that was sintered above 1000°C for more than 24 h. The resultant polycrystalline Nd:YAG powder was melted to grow the Nd:YAG single crystal at temperature from 1970°C to 2100°C in a Czochraski furnace with an iridium crucible (Ø60 mm × 60 mm) and an induction heat system (made by the 26th Institute of Chinese Electronics Technology Group Corporation). The crystal growth is carried out under nitrogen gases. The appropriate initial growth parameters were selected, and to start the growth with the interface shape of the growth interface was convex to the melt. First, the YAG seed crystal was dropped until its end reached the melt surface center at a suitable melt temperature obtained through heat power control. When the seed was not melted and its diameter did not decrease, it was pulled upward with an initial mechanical shift speed 0.6 mm/h and rotated at 8 r/min, which is the shoulder growth stage. It should be noted as the operation details that the shoulder stage has a micro-mechanical pull to the crystal, the rotation speed at the shoulder stage was decreased to 0 r/min from the initial 8 r/min, and the pull speed from the initial 0.6 mm/h to 0.4 mm/h, and

the crystal growth was about 0.4 mm/h. After seven days, the final boule of Nd:YAG single crystal had a diameter of 50 mm, a length of 40 mm, and a weight of ~400 g. The crystal boule was then annealed above 1250°C for ~48 h to remove the interior stress, was cut into rods, and was polished into a laser rod sample.

3. Nd^{3+} CONCENTRATION DISTRIBUTION IN EXPERIMENTAL CRYSTALS

The homemade gradient concentration Nd:YAG crystal rod has a total length of 58 mm (shoulder included), which is cut into sliced samples each with about 5 mm interspace along the axial direction. The measurement of the Nd element content used laser ablation inductively-coupled plasma mass spectrometry (LA-ICP-MS) coupled with a GeoLasPro 193 nm ArF excimer laser ablation system and Agilent 7500a Quadrupole ICP-MS. In the process of laser ablation, helium and argon were used as the carrier and compensation gases respectively to adjust sensitivity. The standard glasses SRM 610 and SRM 612 were used as the reference calibration to quantify the element Nd content. Three random sites were measured at each crystal slice, and the average values of the Nd element concentration along the rod axis were plotted to describe the spatial dependence. As shown in Fig. 1, the concentration of the Nd element gradually increased from 0.34 to 0.80 at.%. The concentration of the Nd element at the front part of the crystal rod increased slowly, but the concentration near the final end increased exponentially with distance. Using a fit to the data, the concentration of Nd^{3+} can be described using

$$n = 0.0223 \exp(l/19) + 0.331, \tag{4}$$

where n is the Nd^{3+} concentration in the crystal and l is the axial position from the end of the crystal.

4. TEMPERATURE DISTRIBUTION AND THERMAL FOCAL LENGTHS

A. Temperature Distribution along the Rod Axis

For crystals with uniform concentration, the Nd^{3+} concentration is a constant, while for crystals with gradually varying concentration, its value changes with the length l. Assume that $\overline{n}$ is the average concentration of the graded crystal, integrating the value of n as a function of the l change, which then gives the average concentration

$$\overline{n}(l_2 - l_1) = \int_{l_1}^{l_2} n\mathrm{d}l. \tag{5}$$

A 40 mm long crystal rod with concentration of 0.39–0.80 at.% was cut from the homemade gradual gradient crystal. By the Eqs. (4) and (5), the average concentration of the gradient crystal rod can be calculated to be 0.55 at.%, which is close to the value of 0.60 at.%. Therefore, the uniformly doped 0.60 at.% crystal rod was used in our experimental research to compare with the gradient concentration crystal rod.

The gradient concentration crystal of 0.39–0.80 at.% and uniform concentration crystal of 0.60 at.% were used to test their temperature distributions under high-repetition-rate pulse pumping. The bottom parts of the crystal rods were in contact with the heat sink that was controlled at 25°C, while the upper parts of the crystal rods were placed in air. The temperature distributions of the crystals were determined using a Flir thermal imaging camera (model T450sc). The pumping power was 45 W (Fig. 2). The maximum infrared temperature at the incident end of the pump light was only 268.3°C for the gradient concentration crystal rod, which was very much lower than that of the uniform concentration crystal (504.1°C). Surprisingly, the values of temperature for the gradient crystal rod and the uniform crystal rod were from 268.3°C to 50.3°C and from 504.1°C to 27.6°C, respectively. The maximum temperature of the gradient concentration crystal rod was only half that of the uniform concentration crystal rod, and the temperature at the end was higher than that of the uniform concentration crystal rod. The results reveal that the gradient concentration crystal rod did not only lower the maximum temperature value but also remarkably exhibited a more even temperature distribution along the rod axis.

To further analyze the temperature distribution along the rod, a temperature value was tested every 5 mm (Fig. 3). For 0.6 at.% uniformly doped crystal, the temperature decrease was very rapid as a function of position along the rod axis. The temperature can be approximated as a quadratic relationship between the temperature distribution and the distance, leading to a correlated distribution of the refractive index and birefringence over the cross section of the rod. This dependence is equivalent to the spherical lens effect [21,22]. The temperature

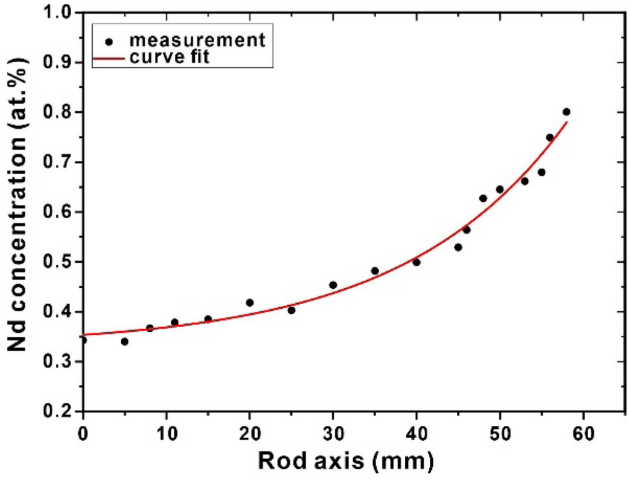

Fig. 1. Nd^{3+} concentration distribution along the crystal rod axis.

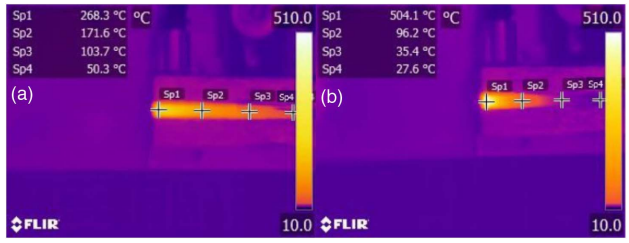

Fig. 2. Different temperature distribution of the two crystal rods under pump power of 45 W. Crystals rod of (a) 0.39–0.80 at.%, (b) 0.60 at.%.

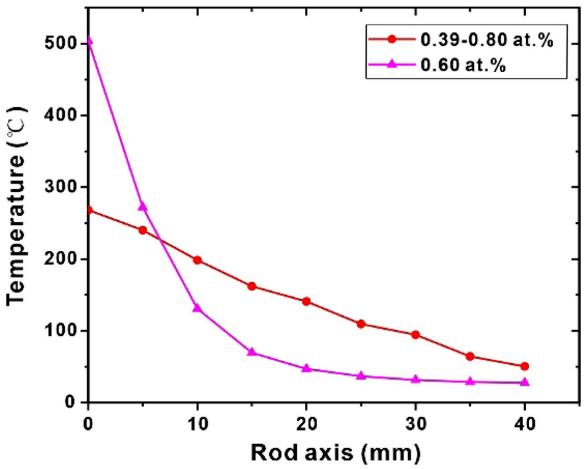

Fig. 3. Different temperature distribution of the rod axis.

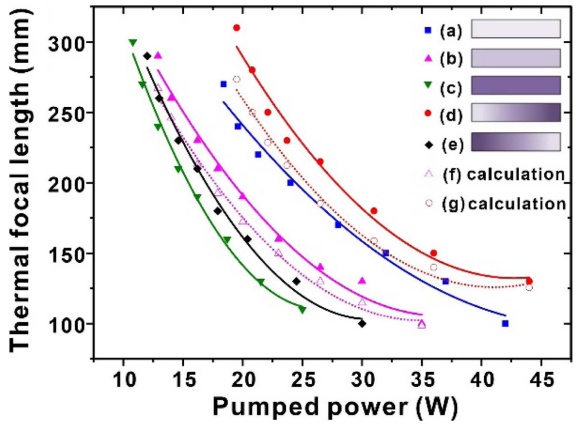

Fig. 4. Dependence of the focal length on the pump power. Different Nd:YAG concentrations of (a) 0.40 at.%, (b) 0.60 at.%, (c) 0.80 at.%, (d) 0.39–0.80 at.%, and (e) 0.80–0.39 at.%. Theoretical calculation of (f) 0.60 at.% and (g) 0.39–0.80 at.%.

distribution of the gradient concentration crystal rod is almost linear along the axial direction. Different from uniform concentration crystal rods, the middle and final part of the crystal rod also absorbs the remaining pump light to generate some heat, making its temperature distribution more uniform and the axial thermal gradient much smaller than that of the uniform concentration crystal rods. That makes the thermal lens effect much smaller for the gradient concentration rods than for the uniform concentration crystal rods.

B. Comparison of Thermal Focal Lengths

The above results proved that the gradient concentration crystal has superior performance of the temperature distribution compared with the uniform concentration crystal. In order to explore the influence on the thermal lensing effect, theoretical calculations were performed in combination with experimental measurements.

Here the thermally induced lens is assumed to be an ideal thin lens. Based on the theorem of light transmission optics, as a consequence, the focal length lens f is given by [23]

$$f = \frac{-r^2}{2\Delta \mathrm{OPD}}. \tag{6}$$

The optical path difference (OPD) can be expressed as [24]

$$\Delta \mathrm{OPD} = \int \frac{\mathrm{d}n}{\mathrm{d}T}[T(r,z) - T(0,z)]\mathrm{d}z + (n_0 - 1)\Delta l(r) + \sum_{i,j=1}^{3} \int \frac{\partial n}{\partial \varepsilon_{i,j}} \varepsilon_{i,j} \mathrm{d}z, \tag{7}$$

where $\frac{\mathrm{d}n}{\mathrm{d}T} = 7.3 \times 10^{-6}\ \mathrm{K}^{-1}$ is the thermo-optical coefficient, $\Delta l(r)$ is the axial end bulging, and $T(r,z)$ is the temperature distribution. The value of $n_0 = 1.82$ is the refractive index. If the pumped surface is coated to be highly reflective, the factor $n_0 - 1$ has to be replaced by n_0. $\frac{\partial n}{\partial \varepsilon_{i,j}}$ is the elastic-optic coefficient, and $\varepsilon_{i,j}$ is the strain tensor [25] of the elastic-optic coefficient [26].

Using Eqs. (6) and (7) and the temperature distribution, the thermal focal length value can be calculated. The curves of (f) and (g), in Fig. 4, show that the calculation results for 0.6 at.% Nd^{3+} uniform concentration crystal rod and 0.39–0.80 at.% Nd^{3+} gradient concentration crystal rod are consistent with their measured values according to the critical cavity stability conditions shown in (b) and (d). It can be seen that the thermal focal length values of different concentration crystals decreased with the increasing pump power. Compared with other crystals, the thermal focal lengths for the high concentration of 0.80 at.% and 0.80–0.39 at.% crystals were smaller, and they became much smaller with the pump power increase as shown in (c) and (e) of Fig. 4. The evolutions of two thermal focal lengths were almost identical because they had the same high Nd^{3+} concentration at their incident end, playing a decisive role in affecting thermal focal length. This was also confirmed from the thermal focal length of the 0.60 at.% crystal, which is larger than the thermal focal length of the 0.80–0.39 at.% crystal with an almost average concentration of 0.60 at.%.

The absorption of pump light is positively correlated with the ion concentration, and the higher concentration results in serious thermal effect under high pump power. Meanwhile, the evolutions of thermal focal lengths of crystal rods with a lower concentration of 0.40 at.% and 0.39–0.80 at.% showed an obvious difference, in which the thermal focal length of the 0.39–0.80 at.% rod is larger as shown in (a) and (b) of Fig. 4. The increasing dopant concentration enhanced the utilization ratio of pump light, which is beneficial for improving the laser conversion efficiency.

5. LASER EXPERIMENTAL SETUP AND RESULT ANALYSIS

A. Laser Experimental Setup

Figure 5 schematically draws the structure of 2 kHz pulse laser using the gradient crystals and uniform crystal rods. The diameters of the five types of crystal rods were 3 mm with the length of 40 mm, and each side of the laser rod was coated to be antireflective at 808 and 1064 nm. The crystals were wrapped with indium foil and were mounted in water-cooled copper heat sinks at 293 K. The laser oscillating configuration was a plane-parallel cavity with the overall length of 90 mm. The flat

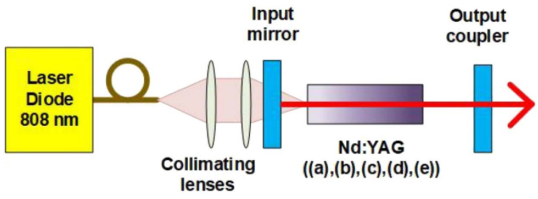

Fig. 5. Experimental arrangement for comparison of the continuously spatially varying and conventional crystals. Schematic configurations for the different Nd:YAG concentrations of (a) 0.40 at.%, (b) 0.60 at.%, (c) 0.80 at.%, (d) 0.39–0.80 at.%, and (e) 0.80–0.39 at.%.

input mirror was coated for high transmission at 808 nm and coated for high reflection at 1064 nm. A flat mirror with a reflectivity of 85% at 1064 nm was utilized as the laser output coupler, which was experimentally found to be with the optimal reflectivity. A fiber-coupled laser diode with a numerical aperture of 0.22 and a core diameter of 400 μm was used as pump source with an emission wavelength of ~808 nm and a maximum output power of 45 W. After the optical coupling system, the spot size of the pump beam imaging in the center of the end face of crystal rod is 800 μm. The experiment was carried out at a repetition rate of 2 kHz, and the pulse duration of pump light was 230 μs. The laser output power was measured using a power meter (Coherent LM-150 FS HTD).

Here we used three uniform crystal rods with different Nd^{3+} contents: 0.40, 0.60, and 0.80 at.% as shown in (a), (b), and (c) of Fig. 5. A gradient crystal rod with 0.39–0.80 at.% was used for this experiment, but the laser performances in two pumping directions were tested with 0.39 at.% and with 0.80 at.% at the incident end, as indicated in (d) and (e) of Fig. 5, respectively.

B. Comparison of Laser Output Power

Figure 6 shows the dependence of the output power at 1064 nm on the pump power at 808 nm for each of the gain media. The pump thresholds for all gain media were found to be almost the same: ~2.7 W. Below the pump power of 18 W, the output power of different Nd^{3+} concentrations of crystal rods was almost identical and exhibited the same increasing rate with pump power. It can be seen that the slope of the increasing output power is different for each crystal rod at the pump power between 18 W and 30 W. The output powers of crystal rods with higher Nd^{3+} concentrations of 0.80 at.% and 0.80–0.39 at.% were very close, and the magnitudes of the increases were smallest. It is indirectly explained that the performances of absorption pump energy and heat generation of the two crystal rods were similar, corresponding to the similarity of the thermal focal lengths (Fig. 4). For crystal rods with Nd^{3+} concentration of 0.40 at.% and 0.39–0.80 at.%, their output powers were higher than those of other crystals. A downward trend in the output power of high Nd^{3+} concentrations of crystals (0.80 at.% and 0.80–0.39 at.%) emerged for the pump power above 30 W. Rods with higher doping concentration and large absorption coefficient made their incident ends absorb more power and produce a great deal of heat by absorbing high pump power. That created a more serious thermal lens effect and resulted in a smaller volume of the fundamental mode of the plane-parallel resonator, accounting for the decrease of output power. At a lower Nd^{3+} concentration of 0.60 at.%, the output laser power showed a very slow increase with greater than 40 W pump power. In contrast, the output laser power of crystals with gradient concentrations of 0.39–0.80 at.% and 0.40 at.% still kept a linear increase, and the gradient concentration crystal had significantly higher output power than the uniform concentration crystal. This can be because the gradient crystal would produce less heat at the incident end, giving a small temperature gradient along the rod axis, thus improving the pump and temperature distributions, and decreasing the thermal lens effect to enhance laser oscillation efficiency.

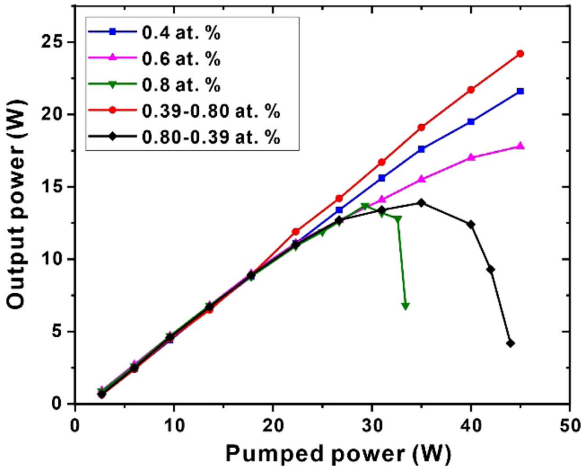

Fig. 6. Output average power with respect to the absorbed pump power for each laser crystal.

As shown in Fig. 6, when the pump light was 45 W, the output laser power of the gradient concentration crystal of 0.39–0.80 at.% was 24.2 W, and its optical-to-optical conversion efficiency was 53.8%, while the uniform concentration crystal of 0.60 at.% gave out a maximal output laser power of only 17.8 W. Here the maximal output power of gradient crystal was greatly enhanced by 35.9% in comparison with the uniform crystal.

The beam propagation analyzer of Spirion (M2-200S-USB) was used to obtain beam profile images and beam qualities. The measured beam quality factors were $M_x^2 = 3.335$ and $M_y^2 = 3.329$ for the gradient concentration crystal of 0.39–0.80 at.%,

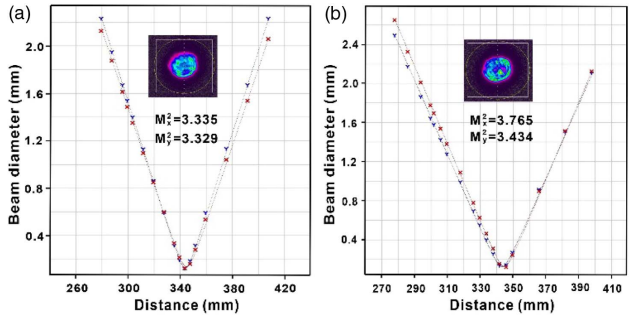

Fig. 7. Beam profiles and beam qualities of (a) 0.39–0.80 at.% and (b) 0.60 at.%.

and the beam quality factors of the uniform concentration crystal of 0.60 at.% were $M_x^2 = 3.765$ and $M_y^2 = 3.434$ (Fig. 7). Their beam profiles were also shown in Fig. 7. The pulse durations of crystals of 0.39–0.80 at.% and 0.60 at.% were 196.1 μs and 191.9 μs, respectively, tested by a detector (Thorlabs DET10A/M).

It should be noted that in order to objectively reflect the temperature characteristics of the gradient concentration crystal rod itself, in this case we did not use the non-dopant crystal cap at the two ends of the experimental crystal rod, limiting the acquisition of greater laser output power. Moreover, the output laser power of gradient concentration crystal is not saturated due to the limitation of the pump source.

6. CONCLUSION

In summary, we have made a gradient concentration Nd:YAG crystal and successfully realized the operation and high-efficiency output of a 2 kHz pulse laser. The gradient concentration crystal exhibited excellent performance in pump and temperature distributions, enhancing the absorption of the middle and final rod end to pump light. These lower the temperature of the incident end, mitigate the temperature gradient along the rod axis, and lead to a weak thermal lensing effect. The maximum output power of gradient crystal was greatly enhanced by 35.9% in comparison with the uniform crystal. Thereby, the gradient dopant crystal is a convenient and practical gain medium to appreciably scale the output power in the end-pumped pulse laser system with high pulse energy and high repetition rate. This represents a performance increase and also offers a way for the future technical route to high energy efficiency. The method used to grow gradient concentration Nd:YAG crystals can also be used for other laser crystals (for example, Nd:GGG, Nd:YAP, and Nd:YVO_4).

Funding. National Key Research and Development Program of China (2018YFB0407204, 2016YFB0701001).

Acknowledgment. The authors express their appreciation to senior fellow Dr. John Lohr of General Atomics of USA for his significant discussions.

Disclosures. The authors declare no conflicts of interest.

Data Availability

Data underlying the results presented in this paper are not publicly available at this time but may be obtained from the authors upon reasonable request.

REFERENCES

1. A. K. Cousins, "Temperature and thermal stress scaling in finite-length end-pumped laser rods," IEEE J. Quantum Electron. **28**, 1057–1069 (1992).
2. Y. Chen, T. Huang, C. Kao, C. Wang, and S. Wang, "Optimization in scaling fiber-coupled laser-diode end-pumped lasers to higher power: influence of thermal effect," IEEE J. Quantum Electron. **33**, 1424–1429 (1997).
3. W. Koechner, "Absorbed pump power, thermal profile and stresses in a cw pumped Nd:YAG crystal," Appl. Opt. **9**, 1429–1434 (1970).
4. T. Y. Fan, "Heat generation in Nd:YAG and Yb:YAG," IEEE J. Quantum Electron. **29**, 1457–1459 (1993).
5. G. Wagner, M. Shiler, and V. Wulfmeyer, "Simulations of thermal lensing of a Ti:sapphire crystal end-pumped with high average power," Opt. Express **13**, 8045–8055 (2005).
6. M. Nadimi, T. Waritanant, and A. Major, "High power and beam quality continuous-wave Nd:$GdVO_4$ laser in-band diode-pumped at 912 nm," Photon. Res. **5**, 346–349 (2017).
7. E. C. Honea, R. J. Beach, S. C. Mitchell, J. A. Skidmore, M. A. Emanuel, S. B. Sutton, S. A. Payne, P. V. Avizonis, R. S. Monroe, and D. G. Harris, "High-power dual-rod Yb:YAG laser," Opt. Lett. **25**, 805–807 (2000).
8. Y. Huang, Y. Huang, H. Liang, K. Su, Y. Chen, and K. Huang, "Comparative study between conventional and diffusion-bonded Nd-doped vanadate crystals in the passively mode-locked operation," Opt. Express **18**, 9518–9524 (2010).
9. D. Kracht, M. Frede, R. Wilhelm, and C. Fallnich, "Comparison of crystalline and ceramic composite Nd:YAG for high power diode end-pumping," Opt. Express. **13**, 6212–6216 (2005).
10. Y. Mao, Y. Gao, and L. Wang, "254 W laser-diode dual-end-pumped Tm:YAP InnoSlab laser," Appl. Opt. **59**, 8224–8227 (2020).
11. Y. Chen, L. Lee, T. Huang, and C. Wang, "Study of high-power diode-end-pumped Nd:YVO_4 laser at 1.34 μm: influence of Auger upconversion," Opt. Commun. **163**, 198–202 (1999).
12. Y. Chen, "Design criteria for concentration optimization in scaling diode end-pumped lasers to high powers: influence of thermal fracture," IEEE J. Quantum Electron. **35**, 234–239 (1999).
13. V. Kushawaha and Y. Chen, "Diode end-pumped high-efficiency Nd:YAG laser," Appl. Phys. B **59**, 659–661 (1994).
14. M. Frede, D. Kracht, M. Engelbrecht, and C. Fallnich, "Compact high-power end-pumped Nd:YAG laser," Opt. Laser Technol. **38**, 183–185 (2006).
15. R. Wilhelm, D. Freiburg, M. Frede, and D. Kracht, "End-pumped Nd:YAG laser with a longitudinal hyperbolic dopant concentration profile," Opt. Express **16**, 20106–20116 (2008).
16. R. Wilhelm, M. Frede, and D. Kracht, "Power scaling of end–pumped solid–state rod lasers by longitudinal dopant concentration gradients," IEEE J. Quantum Electron. **44**, 232–244 (2008).
17. A. M. Rodin, M. Grishin, and A. Michailovas, "Picosecond laser with 11 W output power at 1342 nm based on composite multiple doping level Nd:YVO_4 crystal," Opt. Laser Technol. **76**, 46–52 (2016).
18. Q. Shen, X. Cui, M. Yan, U. Eismann, T. Yuan, W. Zhang, C. Peng, Y. Chen, and J. Pan, "11-watt single-frequency 1342-nm laser based on multi-segmented Nd:YVO_4 crystal," Opt. Express **27**, 31913–31925 (2019).
19. Q. Zhang, S. Yin, D. Sun, and W. Ming, "Segregation during crystal growth from melt and absorption cross section determination by optical absorption method," Sci. China Phys. Mech. **51**, 481–491 (2008).
20. V. V. Galutskiy, M. I. Vatlina, and E. V. Stroganova, "Growth of single crystal with a gradient of concentration of impurities by the Czochralski method using additional liquid charging," J. Cryst. Growth **311**, 1190–1194 (2009).
21. H. Kogelnik, "Imaging of optical modes—resonators with internal lenses," Bell Syst. Tech. J. **44**, 455–494 (1965).
22. H. Eichler, A. Haase, R. Menzel, and A. Siemoneit, "Thermal lensing and depolarization in a highly pumped Nd:YAG laser amplifier," J. Phys. D **26**, 1884–1891 (1993).
23. W. Roger, B. Neuenschwander, M. M. Donald, M. B. Roos, and H. Weber, "Cooling schemes for longitudinally diode laser-pumped Nd:YAG rods," IEEE J. Quantum Electron. **34**, 1046–1053 (1998).
24. X. Peng, L. Xu, and A. K. Asundi, "Thermal lensing effects for diode-end-pumped Nd:YVO_4 and Nd:YAG lasers," Opt. Eng. **43**, 2454–2461 (2004).
25. W. Koechner and D. Rice, "Effect of birefringence on the performance of linearly polarized YAG:Nd lasers," IEEE J. Quantum Electron. **6**, 557–566 (1970).
26. W. Koechner, *Solid-State Laser Engineering* (Springer-Verlag, 1992).